ROYAL SOCIETY
OF CHEMISTRY

EDGE ARTICLE

Check for updates

All publication charges for this article have been paid for by the Royal Society of Chemistry

Coordinating zincophilic sites and a solvation shell for a dendrite-free Zn anode under the synergistic effects of polyacrylonitrile and dimethyl sulfoxide†

Zhenjie Liu, ‡[a] Jiale Ma, ‡[b] Xiangjian Liu,[c] Haiyang Wu,[d] Dianlun Wu,[a] Bin Chen,[a] Peng Huang,[d] Yang Huang, *[a] Lei Wang,[a] Zhenyu Li *[b] and Shulei Chou *[e]

The advantages of aqueous zinc-ion batteries (AZIBs) are largely offset by the dendrite growth on the Zn anode, which is induced by the heterogeneous electrical field and limited ion transport of the Zn anode–electrolyte interface during plating and stripping. Here, we propose a dimethyl sulfoxide (DMSO)–H_2O hybrid electrolyte containing polyacrylonitrile (PAN) additives (PAN–DMSO–H_2O) to improve the electrical field and ion transport of the Zn anode, which can thus effectively inhibit dendrite growth. Experimental characterization and theoretical calculations show that PAN preferentially adsorbs on the Zn anode surface and provides abundant zincophilic sites after its solubilization by the DMSO, enabling a balanced electric field and lateral Zn plating. DMSO regulates the solvation structure of the Zn^{2+} ions and strongly bonds to H_2O, which concurrently reduces side reactions and enhances the ion transport. Thanks to the synergistic effects of PAN and DMSO, the Zn anode presents a dendrite-free surface during plating/stripping. Moreover, Zn–Zn symmetric and Zn–$NaV_3O_8 \cdot 1.5H_2O$ full batteries with this PAN–DMSO–H_2O electrolyte achieve enhanced coulombic efficiency and cycling stability compared to those with a pristine aqueous electrolyte. The results reported herein will inspire other electrolyte designs for high-performance AZIBs.

Introduction

Aqueous zinc-ion batteries (AZIBs) are attracting increasing attention due to their high level of safety, relatively low price, pollution-free properties, *etc*.[1–4] For most AZIBs, metallic zinc (Zn) is used directly as an ideal anode material,[5–7] with the benefits of a high theoretical capacity (821 mA h g^{-1}), low redox potential (-0.76 V *vs.* standard hydrogen electrode, SHE) and inherent abundance.[8–10] Similar to the alkali metal anodes in lithium and sodium batteries,[11,12] the Zn anode is oxidized to

Zn^{2+} ions upon discharge, and these Zn^{2+} ions are reversibly electroplated on the Zn anode upon charging. In traditional aqueous electrolytes, the Zn anode inevitably has dendrite growth due to the heterogeneous nucleation and disordered growth during Zn electroplating, leading to the formation of dead Zn, poor coulombic efficiency and even battery short-circuiting.[13–15] Simultaneously, some undesirable side reactions, such as the hydrogen evolution reaction (HER) and Zn corrosion, occur on the Zn anode, further degrading its structural stability.[16–18] Thus, the performances of AZIBs are unexpectedly diminished, and they exhibit low capacity, short cycle life, *etc*.

Fundamental research into AZIBs indicates that a heterogeneous electrical field results in random Zn nucleation, while limited ion transport leads to inhomogeneous Zn growth, both of which accelerate dendrite growth and intensify side reactions.[14,15] Recently, besides Zn anode modification,[19–21] the development of new electrolytes has proved to be a convenient and cost effective way to improve the electrical field and ion transport of the Zn anode, which enables the achievement of high-performance AZIBs.[22] The proposed strategies can be roughly divided into two groups: additive introduction and co-solvent electrolyte engineering. As for additive introduction, much research focuses on the application of organics, including organic ions,[23–27] small organic molecules,[28–33] and

[a] Shenzhen Key Laboratory of Polymer Science and Technology, College of Materials Science and Engineering, Shenzhen University, Shenzhen 518055, Guangdong, China. E-mail: y.huang@outlook.com; yanghuang@szu.edu.cn

[b] Hefei National Research Center for Physical Sciences at the Microscale, University of Science and Technology of China, Hefei 230026, Anhui, China. E-mail: zyli@ustc.edu.cn

[c] School of Chemistry and Chemical Engineering, Beijing Institute of Technology, Beijing, 100081, China

[d] School of Chemistry and Materials Chemistry, Jiangsu Normal University, Xuzhou, 221116, Jiangsu, China

[e] Institute for Carbon Neutralization, College of Chemistry and Materials Engineering, Wenzhou University, Wenzhou 325035, Zhejiang, China. E-mail: chou@wzu.edu.cn

† Electronic supplementary information (ESI) available. See DOI: https://doi.org/10.1039/d2sc06276c

‡ These authors contributed equally.

polymers.[34–39] These additives adsorb on the Zn anode surface and serve as zincophilic sites to relieve the electron/ion accumulation of zinc seeds, which benefits a homogenous electrical field and prevents the random nucleation of Zn. As for co-solvent electrolyte engineering, many organic solvents have been applied.[40–44] They manipulate the primary solvation shell of Zn^{2+} ions and affect the ion transport rate, which not only promotes orderly Zn electroplating but also inhibits water-associated side reactions. Because the roles of additive introduction and co-solvent electrolyte engineering in improving the stability of the Zn anode are quite different and do not interfere with each other, it is theoretically feasible to combine these two mainstream strategies together and harness their respective advantages to achieve a dendrite-free Zn anode. However, few attempts have been made at this promising approach, wasting the potential of electrolyte development for high-performance AZIBs.

Herein, we have successfully achieved a dendrite-free Zn anode for highly stable AZIBs *via* combining a polyacrylonitrile (PAN) additive with a dimethyl sulfoxide–water hybrid electrolyte (PAN–DMSO–H_2O). Although PAN can effectively inhibit the dendrite growth in AZIBs while serving as a separator[45] or artificial coating,[46] the application potential of PAN as an additive is severely restricted owing to its insolubility in an aqueous electrolyte. To solve this problem, DMSO is used in the electrolyte. DMSO, as an aprotic solvent, can improve the solubilization of PAN molecules due to its incorporation of both hydrophilic and hydrophobic moieties. After their successful dissolution, PAN molecules could preferentially and strongly adsorb on the Zn anode and provide zincophilic sites at the anode–electrolyte interface. Meanwhile, the typical Zn^{2+} solvation sheath is also regulated by the preferential solvation of DMSO molecules. As a result, a uniform electric field and enhanced ion transport at the Zn anode–electrolyte interface can be concurrently realized, which smooths the plating/stripping process and enables a dendrite-free anode surface. Thanks to the synergistic effects of PAN and DMSO, the Zn–Zn symmetric battery containing this PAN–DMSO–H_2O electrolyte shows a better cycle life (>1200 h) and higher coulombic efficiency (99.18%) under a current density of 5.0 mA h cm^{-2}, while a limited cycle life (<5 h) and low coulombic efficiency (89.16%) are obtained in the pristine aqueous electrolyte. Moreover, when coupled with a $NaV_3O_8 \cdot 1.5H_2O$ (NVO) cathode, the Zn–NVO full battery exhibits enhanced cycle stability (over 300 cycles) and high capacity retention (81.1%). Our work should inspire other functional electrolyte design for dendrite-free AZIBs with enhanced stability.

Results and discussion

As an organic macromolecular polymer, PAN is insoluble in the pristine aqueous electrolyte. After the introduction of DMSO, the solubility of PAN is improved, which is due to the effect of the strong hydrophobic (–CH_3) and highly hydrophilic (O=S) moieties of DMSO.[47,48] Specifically, as shown in Fig. S1,† PAN is gradually and then completely dissolved in the PAN–DMSO–

H_2O electrolyte when the volume content of DMSO increases from 20 to 70%. However, when the volume content of DMSO increases to 100%, *i.e.* DMSO replaces water completely, the Zn salt (*i.e.* Zn(OTF)$_2$) in the electrolyte is clearly precipitated. The ion conductivities of the hybrid electrolytes with different amounts of DMSO were measured by AC impedance spectroscopy as shown in Fig. S2.† The results demonstrate that the ionic conductivity gradually decreases with an increase of the DMSO content, since excess DMSO molecules could increase the Zn^{2+} solvation sheath radii and the viscosity of the electrolyte.[40] Therefore, to achieve a balance between good PAN solubility and high ionic conductivity, the volume ratio of DMSO to H_2O in the PAN–DMSO–H_2O electrolyte was set at 1 : 1. If not otherwise specified, the following batteries were all assembled with electrolytes using this optimized volume ratio.

To visualize the dendrite growth, we first investigated the plating process of the Zn anode using an optical microscope with *in situ* setups.[49] As expected, a large number of Zn dendrites grew rapidly in the pristine aqueous electrolyte with a current density of 5.0 mA cm^{-2} (Fig. 1a), which is mainly due to charge-concentration occurring at the tips of the Zn nuclei. Simultaneously, a large amount of gas evolution can be clearly observed owing to the rapid occurrence of the HER (Fig. S3†). The addition of DMSO can effectively decrease the activity of the solvated H_2O and consequently inhibit the related side reactions (*e.g.* the HER),[42] but it cannot completely suppress the formation of Zn dendrites (Fig. 1b). In sharp contrast to the morphological results shown in Fig. 1a and b, a dendrite-free Zn anode is achieved in the PAN–DMSO–H_2O electrolyte, as shown in Fig. 1c. Such apparent differences clearly indicate the effective roles of the PAN additive in solving the Zn dendrite growth problem.

To further study the microstructure evolution, we investigated the surface morphologies of the Zn anodes after the plating process using a scanning electron microscope (SEM), as shown in Fig. S4a–c.† With the PAN–DMSO–H_2O electrolyte, the surface of the plated Zn anode is smooth and homogeneous, whereas the surfaces become rough and inhomogeneous with some obvious voids and bumps after plating in the other two electrolytes, especially in the pristine aqueous electrolyte. Interestingly, the surface morphological differences between the Zn anodes when using the different electrolytes are even greater after the stripping process, as shown in Fig. S4d–f.† Specifically, when using a pristine aqueous electrolyte, the Zn anode has a more inhomogeneous surface compared with those when using DMSO–H_2O or PAN–DMSO–H_2O electrolytes, showing many scattered and dispersed Zn flakes. Such obvious protuberances can aggravate the charge-concentration and facilitate dendrite growth during the following plating process.[50] Moreover, as shown in the transmission electron microscope (TEM) and selected area electron diffraction images in Fig. S5,† the Zn anode has more smaller Zn grains (clusters) after plating in the PAN–DMSO–H_2O electrolyte. This agrees well with the X-ray diffraction (XRD) results (Fig. S6†), in which the full width at half maximum of the XRD peaks in the PAN–DMSO–H_2O electrolyte, an indicator of the grain size, is larger than those in the other two electrolytes. Therefore, the
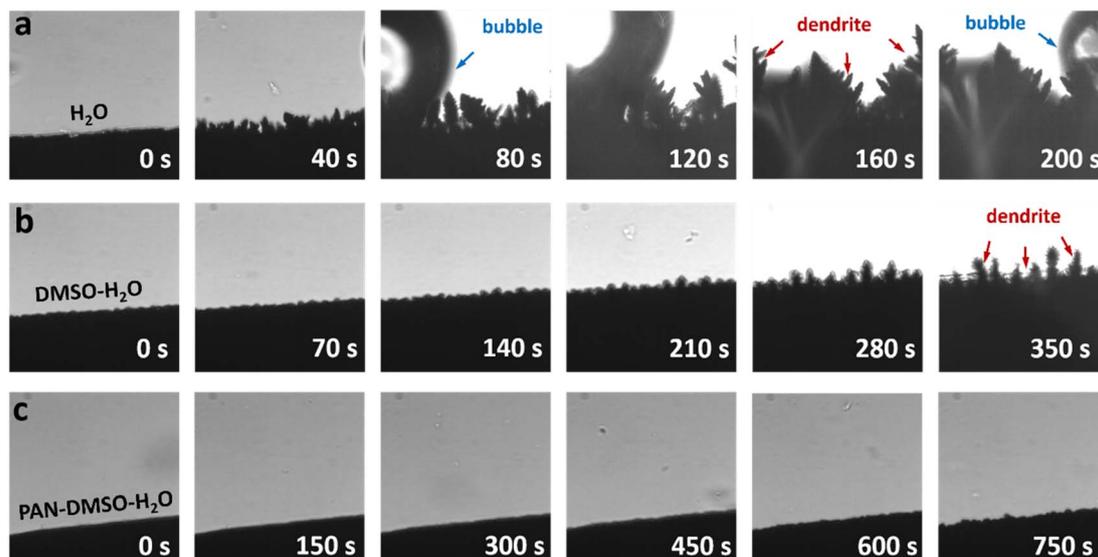
Fig. 1 *In situ* side views of the Zn anodes in different electrolytes during the plating process: (a) pristine aqueous, (b) DMSO−H$_2$O and (c) PAN−DMSO−H$_2$O electrolytes.

application of the PAN additive can result in a smaller initial nucleus and subsequently promote the lateral growth rather than the longitudinal growth of Zn grains (clusters),[51] which enables a smooth and dendrite-free surface after the Zn plating, as shown in Fig. 1c.

To better understand the advantages of the PAN additive in stabilizing the Zn anode during plating/stripping, density functional theory (DFT) calculations were employed to investigate the interactions between the Zn anode, Zn^{2+} ions, and H$_2$O, DMSO and PAN molecules. Fig. 2a shows the adsorption energies (E_{ads}) of H$_2$O, DMSO and PAN on the Zn anode. It was found that the E_{ads} of PAN is much lower (-1.73 eV) than those of H$_2$O (-0.26 eV) and DMSO (-0.63 eV), suggesting its preferential adsorption on the Zn anode. This advantage allows PAN to isolate H$_2$O from the Zn surface, thus prohibiting side reactions (*e.g.* corrosion). The charge density differences between the adsorption configurations of H$_2$O, DMSO and PAN on the Zn anode are also shown in Fig. 2c. A number of electrons transfer from the –N group of PAN to the Zn surface and thus a stable N–Zn bond is constructed, indicating strong chemisorption between PAN and the Zn anode. More importantly, DFT calculations show that the adsorbed PAN matches well with the lattice of the Zn (0001) facet, which ensures an increased formation of N–Zn bonds and thus an improved binding strength between PAN and Zn. In contrast, only a few electrons transfer from H$_2$O or DMSO to the Zn surface. Such weak chemisorption is not helpful to relieve the charge-concentration occurring at the tip of the Zn nuclei and prevent rapid Zn dendrite growth. From the binding energy results shown in Fig. 2b, it is clear that the Zn^{2+} ion prefers to combine with PAN than H$_2$O and DMSO, because the binding energy of Zn^{2+}–PAN (-0.19 eV) is lower than those of Zn^{2+}–H$_2$O (-0.07 eV) and Zn^{2+}–DMSO (-0.11 eV). Therefore, the adsorbed PAN can act as a zincophilic site and favor ordered Zn nucleation.

Also of note is that the adsorption energy of PAN per unit area (-0.86 eV) is much lower than that of DMSO (-0.63 eV), as shown in Fig. S7.† Thus, compared to DMSO–H$_2$O, the lower adsorption energy of PAN–DMSO–H$_2$O enables a stronger interaction between the electrolyte and electrode, which results in better wettability. As shown in the contact angle measurements shown in Fig. S8,† the addition of PAN increases the contact area between the electrode and electrolyte, which is beneficial for Zn^{2+} ion diffusion at the Zn anode–electrolyte interface. In addition to the significant contributions from PAN, DMSO plays important roles in inhibiting side reactions by regulating the Zn^{2+} solvation sheath, which is also good for Zn anode stability.[41] We further investigated the solvation structure of the Zn^{2+} ions in our new electrolyte *via* Raman spectra, Fourier transform infrared spectroscopy (FTIR) and ^{67}Zn nuclear magnetic resonance spectroscopy (NMR) to uncover the specific roles of DMSO (Fig. 2d–f). As shown in the Raman spectra (Fig. 2d), similar to in previous research,[40,41] due to the strong Zn^{2+}–DMSO interaction, the S=O stretching vibration exhibits an obvious shift to a lower wavenumber, while the C–S and C–S–C stretching vibrations shift towards a higher wavenumber.[52] These shifts are attributed to the reconstructed S=O···H–O hydrogen bonds in the electrolyte, simultaneously weakening the interactions between the Zn^{2+} ions and H$_2$O. This is corroborated by the changes in the FTIR results (Fig. 2e). Meanwhile, compared with the pristine aqueous electrolyte, the ^{67}Zn NMR spectrum of the DMSO–H$_2$O electrolyte exhibits a downshift (Fig. 2f), offering further proof for the participation of DMSO in the Zn^{2+} solvation. Thus, the numbers of coordinated H$_2$O molecules around the Zn^{2+} ions are reduced, which favors the prohibition of the HER on the Zn anode surface. Moreover, although the solubilization of PAN is clearly improved by DMSO, PAN cannot actually participate in the regulation of the solvation structure of the Zn^{2+} ions, because
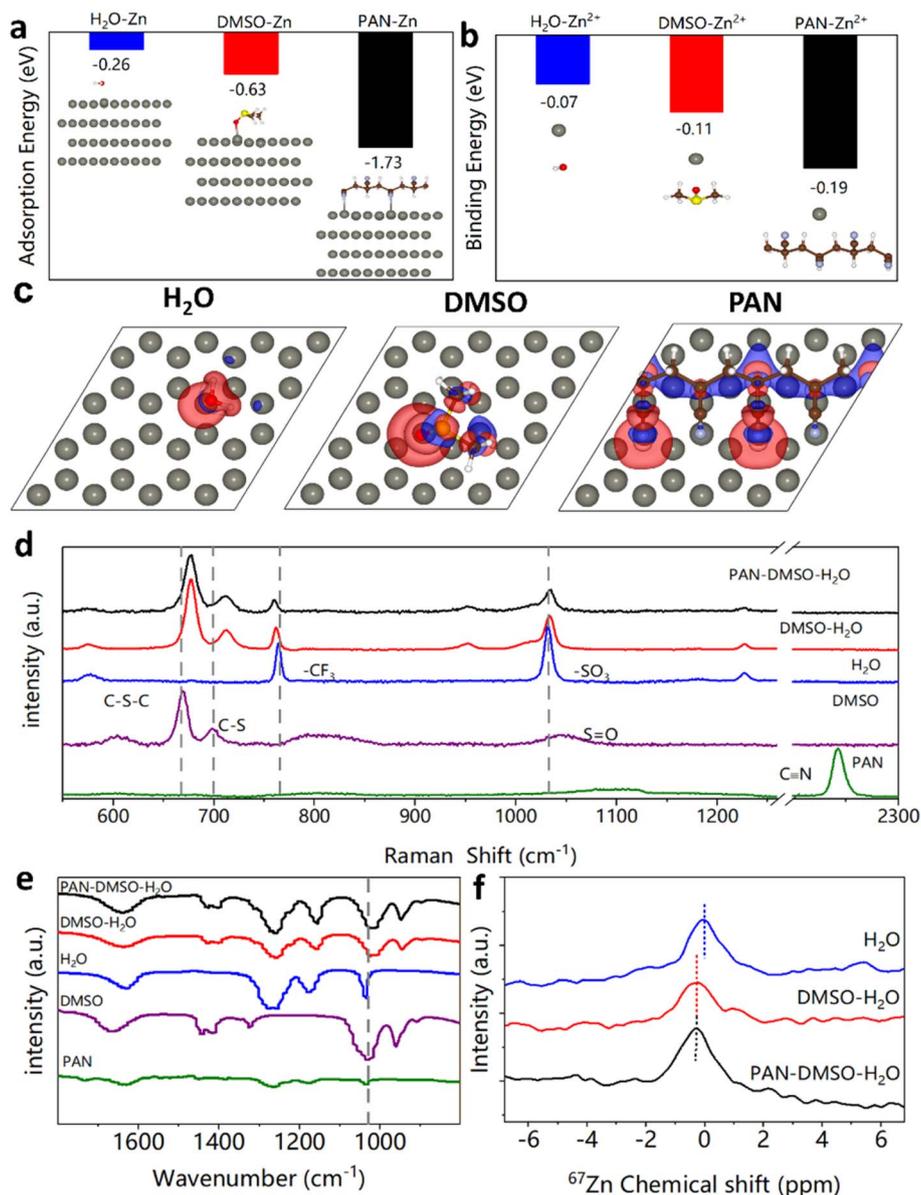
Fig. 2 (a) Comparison of the adsorption energies of H_2O, DMSO and PAN molecules on the Zn anode. The insets show the corresponding adsorption models. (b) Binding energies of Zn^{2+} ions with H_2O, DMSO and PAN molecules from DFT calculations. (c) Vertical views of the charge density differences for H_2O, DMSO and PAN on the Zn anode. (d) Raman and (e) FTIR spectra of the pristine aqueous (blue line), DMSO–H_2O (red line) and PAN–DMSO–H_2O (black line) electrolytes. (f) NMR spectra of ^{67}Zn in three different electrolytes.

the addition of PAN did not continually cause a chemical shift in the ^{67}Zn spectrum in the NMR test (Fig. 2f). This result is consistent with the low degree of complexation between the CN group and Zn^{2+} ions, as reported in a previous study.[53] Therefore, by combining the different and effective roles of PAN and DMSO, the PAN–DMSO–H_2O electrolyte can effectively suppress both Zn dendrite growth and side reactions during Zn plating, as shown in Fig. 1.

Because the formed dendrites are easily separated from the Zn anode (i.e. they become dead Zn), they can further intensify the side reactions and cause performance degradation. To verify this, we investigated the Tafel curves of the Zn anodes with the three electrolytes after resting for one day, and then evaluated

their resistance to side reactions as shown in Fig. S9a.† The anode using the PAN–DMSO–H_2O electrolyte exhibits a reduced corrosion current density compared with those when using the other two electrolytes. This indicates that the smooth anode surface resulting from the synergistic effects of PAN and DMSO can better impede the corrosion reaction and benefit the cyclability of AZIBs. In addition, the by-products (e.g. ZnO) resulting from the corrosion reaction will further impede the transport of Zn^{2+} ions. Thus, we believe the Zn anode in the PAN–DMSO–H_2O electrolyte should have a better ion transport capability. This inference can be proved by electrochemical impedance spectroscopy (EIS) as shown in Fig. S9b,† in which

the interfacial impedance of the Zn anode in the PAN–DMSO–H_2O electrolyte is lower than in the other electrolytes.

We then assembled Zn–Ti batteries to further explore the sustainability, reversibility and average coulombic efficiency of Zn plating/stripping with different electrolytes. As shown in Fig. S10a,† the cyclic voltammetry (CV) curves of the PAN–DMSO–H_2O electrolyte remain almost unchanged, while the curve shapes of the pristine aqueous and DMSO–H_2O electrolytes deteriorate severely. The distinct differences in the CV curves signify that the addition of PAN can prohibit side reactions and improve the reversibility of Zn plating/stripping. Significantly, the nucleation overpotential in the PAN–DMSO–H_2O electrolyte decreases by approximately 120 mV compared to that of the pristine aqueous electrolyte (Fig. 3a), indicating faster reaction kinetics for Zn^{2+} deposition on the Zn anode. Similar phenomena can be observed for the Zn–Zn symmetric battery (Fig. 3b), owing to a lower Zn deposition barrier in PAN–DMSO–H_2O. Additionally, chronoamperometry characterization confirms the positive effects of the PAN additive on Zn nucleation and growth (Fig. 3c). In the pristine aqueous electrolyte, the current density continuously increases, suggesting rampant 2D diffusion along the Zn surface.[54,55] This will lead to the production of Zn dendrites, because so many Zn^{2+} ions preferentially accumulate at the energetically favorable sites. By contrast, in the PAN–DMSO–H_2O electrolyte, the 2D diffusion on the Zn anode surface is quickly disrupted due to the adsorption of DMSO and PAN, resulting in constant 3D diffusion. In this case, the Zn^{2+} ions on the zincophilic sites are locally and rapidly reduced to Zn, forming a dendrite-free surface,[56] which is beneficial to improve the Coulomb

efficiency and stability of the Zn anode. As observed in Fig. 3d and S10b,† the batteries with the pristine aqueous and DMSO–H_2O electrolytes soon experience unstable cycles of plating/stripping and are eventually short-circuited after 11 and 207 cycles, respectively. In comparison, the battery with the PAN–DMSO–H_2O electrolyte remains stable for over 600 cycles and achieves a higher average coulombic efficiency of 99.18%. This improved coulombic efficiency is attributed to the decreased dendrite growth and side reactions at the Zn anode–electrolyte interface.

Benefiting from such a dendrite-free Zn anode, the Zn–Zn symmetric batteries in the PAN–DMSO–H_2O electrolyte exhibit a long cycle stability (more than 1200 h) and a small polarization voltage (less than 0.08 V) at a current density of 5.0 mA cm^{-2}, as shown in Fig. 3e. In contrast, the symmetric batteries in both the pristine aqueous and DMSO–H_2O electrolytes exhibit poor cycle stability (less than 200 h), and either are suddenly short-circuited or experience an increasing voltage polarization during the cycling test. When the current density is decreased to 2.5 mA cm^{-2}, these symmetric batteries exhibit similar trends (Fig. S11†), suggesting the dendrite growth and side reactions seriously damage the cycle stability of the batteries as usual. The Zn anodes in the Zn–Zn symmetric batteries after 100 cycles of plating/stripping under 5.0 mA cm^{-2} were examined using SEM in order to investigate their structural changes. With the pristine aqueous electrolyte, the Zn anode surface is covered with numerous large and sharp protrusions (Fig. 4a and S12a†), while discontinuous fragments and large local hollows are seen for the Zn anode when using the DMSO–H_2O electrolyte (Fig. 4b and S12b†). In comparison,
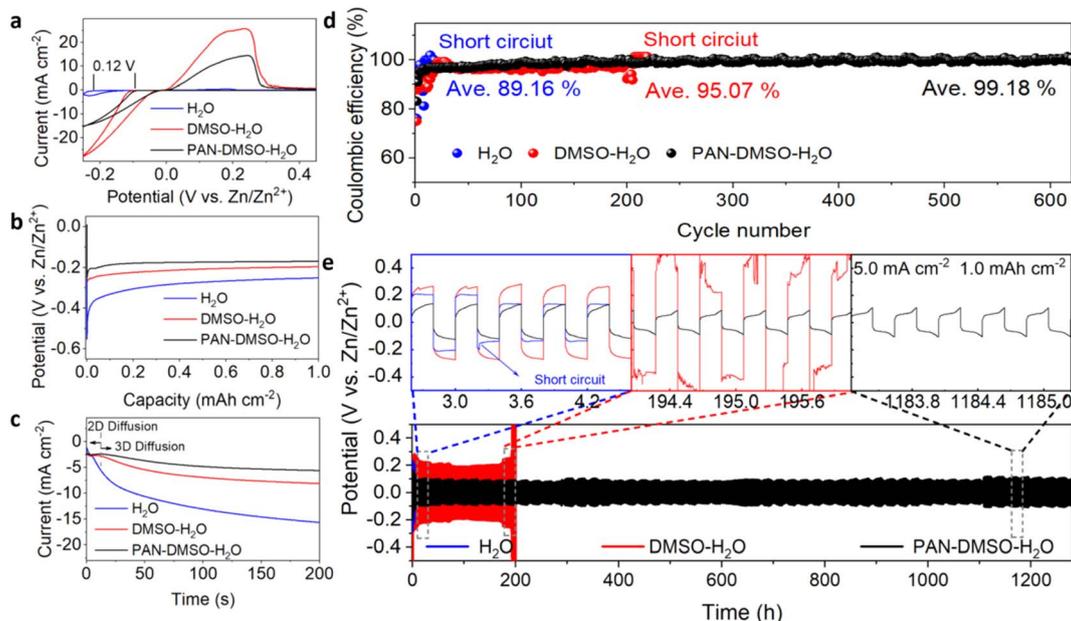

Fig. 3 (a) Cyclic voltammetry curves for Zn plating/stripping in different electrolytes at a scan rate of 1.0 mV s^{-1}. (b) Nucleation over-potential for Zn–Zn symmetric batteries and (c) potentiostatic current–time transient curves of the Zn electrodes in different electrolytes measured at −150 mV. (d) coulombic efficiency of Zn–Ti batteries in different electrolytes. (e) Cycling performance of Zn–Zn symmetric batteries containing different electrolytes at a current density of 5.0 mA cm^{-2} and an areal capacity of 1.0 mA h cm^{-2}. The blue, red and black lines represent the pristine aqueous, DMSO−H_2O and PAN−DMSO−H_2O electrolytes, respectively.
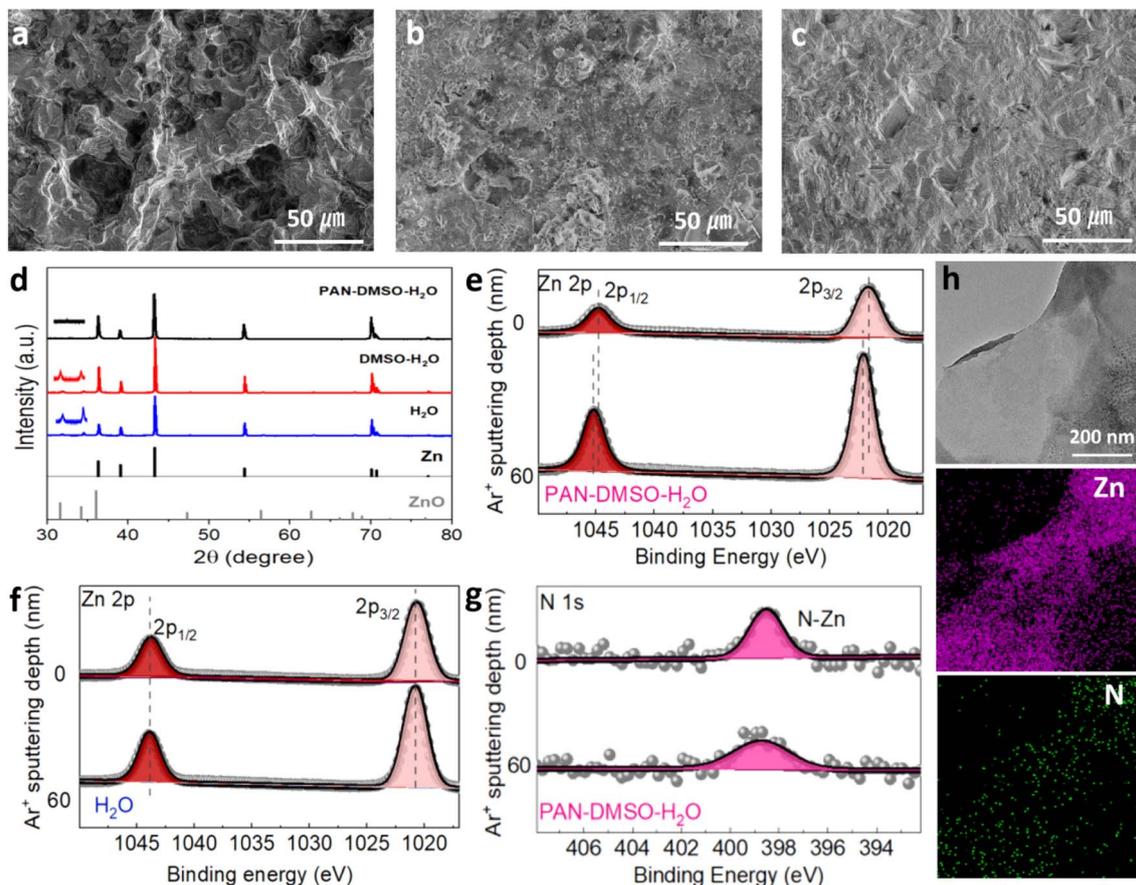
Fig. 4 SEM images of the Zn anode in the (a) pristine aqueous, (b) DMSO−H$_2$O and (c) PAN−DMSO−H$_2$O electrolyte, respectively. (d) XRD patterns and (e and f) Zn 2p and (g) N 1s XPS spectra of the cycled Zn anodes. The Zn anodes harvested from the Zn−Zn symmetric batteries were cycled at 5.0 mA cm^{-2} for 100 cycles. (h) TEM image of a Zn particle that was peeled off from the Zn anode cycled in the PAN−DMSO−H$_2$O electrolyte, and the corresponding energy dispersive X-ray mapping of the Zn and N elements.

the Zn anode can achieve a uniform and neat interface with the PAN−DMSO−H$_2$O electrolyte (Fig. 4c and S12c†). When combined with the cycling test results presented in Fig. 3e, it is convincing that the cycle stability of the Zn anode–electrolyte interface has been greatly enhanced under the synergistic effects of PAN and DMSO.

To uncover the chemical composition changes of the cycled Zn anode, we further examined representative samples using XRD (Fig. 4d) and X-ray photoelectron spectroscopy (XPS, Fig. 4e–g). The characteristic peaks of ZnO are clearly observed in the XRD profiles for both the pristine aqueous and DMSO−H$_2$O electrolytes, which is due to the partial corrosion of the Zn anode from severe side reactions, as indicated in Fig. S9a.† Nevertheless, there is hardly any evidence of ZnO diffraction peaks in the PAN−DMSO−H$_2$O electrolyte sample. However, as shown in the XPS data in Fig. 4e, the Zn 2p spectrum of the Zn anode cycled in the PAN−DMSO−H$_2$O electrolyte exhibits two peaks at 1021.6 and 1044.7 eV, which are ascribed to Zn 2p$_{3/2}$ and Zn 2p$_{1/2}$ of Zn^{2+}, respectively.[26,57]

After Ar$^+$ etching at a depth of 60 nm, these two peaks shifted to 1022.1 and 1045.3 eV, revealing the metallic state of Zn^0 (Fig. 4e).[58,59] Thus, we assume that due to the protection by PAN,

only a shallow layer of the Zn anode is oxidized from the side reactions during repeated plating/stripping. In comparison, the Zn 2p spectrum of the anode cycled in the pristine aqueous or DMSO−H$_2$O electrolyte either exhibits no differences or fewer variations before and after Ar$^+$ etching (Fig. 4f and S13†), indicating a deeper growth of ZnO resulting from the severe corrosion by the side reactions. More importantly, as shown in the N 1s spectra of the anode cycled in the PAN−DMSO−H$_2$O electrolyte (Fig. 4g), a strong N peak appears at 398.5 eV.[60] This could be a clear signature of the chemical adsorption of PAN on the Zn anode, considering that PAN is stable during Zn plating/ stripping (Fig. S14†). After deep Ar$^+$ etching of 60 nm, a similar N peak still exists, as shown in Fig. 4g, suggesting that PAN not only simply adsorbs on the Zn anode but also strongly integrates into the plated Zn. The existence of N is further confirmed by the energy dispersive X-ray (EDS) mapping of the Zn particles that have peeled off from the corresponding Zn anode. The N signals are widely distributed across the sample, as are the Zn signals (Fig. 4h). The above results illustrate that PAN can strongly bond with the Zn anode *via* its N-sites, which is favorable for inhibiting the dendrite growth as discussed below.

In light of the above theoretical and experimental results, we propose the specific roles of the PAN–DMSO–H$_2$O electrolyte in suppressing Zn dendrite growth and side reactions as shown in Fig. 5a. In the pristine aqueous electrolyte, more water molecules are dissociated in a free state with high activity, which can result in close contact with the Zn anode and induce serious corrosion reactions. Meanwhile, Zn^{2+} ions in the electrolyte will readily accumulate at the tip on the rough Zn anode due to a nonuniform electric field, resulting in the rapid growth of Zn dendrites as shown in the left diagram of Fig. 5a. In contrast, thanks to the synergistic effects of PAN and DMSO, a smooth and dendrite-free Zn anode can be achieved in the PAN–DMSO–H$_2$O electrolyte. First, the adsorbed PAN can realize a balanced electric field on the anode surface and further relieve the tip effects (as shown in the right diagram of Fig. 5a), due to its strong interaction with the Zn anode *via* the N–Zn bond, as shown in Fig. 5b. Second, the adsorbed PAN can act as zincophilic sites for guiding the uniform deposition during the following nucleation process, owing to the high binding energy between the PAN and Zn^{2+} ions. The presence of these abundant zincophilic sites facilitates lateral growth rather than longitudinal growth of Zn, leading to a smooth plating surface. Third, the concurrent addition of DMSO can regulate the solvation

sheath of the Zn^{2+} ions and enhance the ion transport at the anode–electrolyte interface, which not only reduces the side reactions but also ensures uniform nucleation and growth of the Zn plating. As a result, the Zn anode could exhibit a dendrite-free surface during repeated stripping/plating in the PAN–DMSO–H$_2$O electrolyte.

In order to demonstrate the practicability of the PAN–DMSO–H$_2$O electrolyte, a full battery was assembled using NVO as the cathode. Before assembling the Zn–NVO full battery, we first examined the electrochemical stabilization window of the electrolytes using linear sweep voltammetry, as shown in Fig. S15.† The onset voltage of the H$_2$ evolution reaction and the corresponding current response suggest that the PAN–DMSO–H$_2$O electrolyte can effectively inhibit the production of H$_2$. As shown in Fig. 5c, the Zn–NVO full batteries exhibited similar CV curves in different electrolytes, but a negative shift of the reduction peaks occurs in the DMSO–H$_2$O electrolyte due to the strong solvation of DMSO.[41,61] Fig. 5d and e show the cycling performance of the full batteries at a current density of 1.0 A g^{-1} and the corresponding galvanostatic charge–discharge curves. The full battery with the PAN–DMSO–H$_2$O electrolyte can realize an initial capacity of 189.8 mA h g^{-1} and a high capacity retention rate (81.1%) after 300 cycles. In contrast, the full
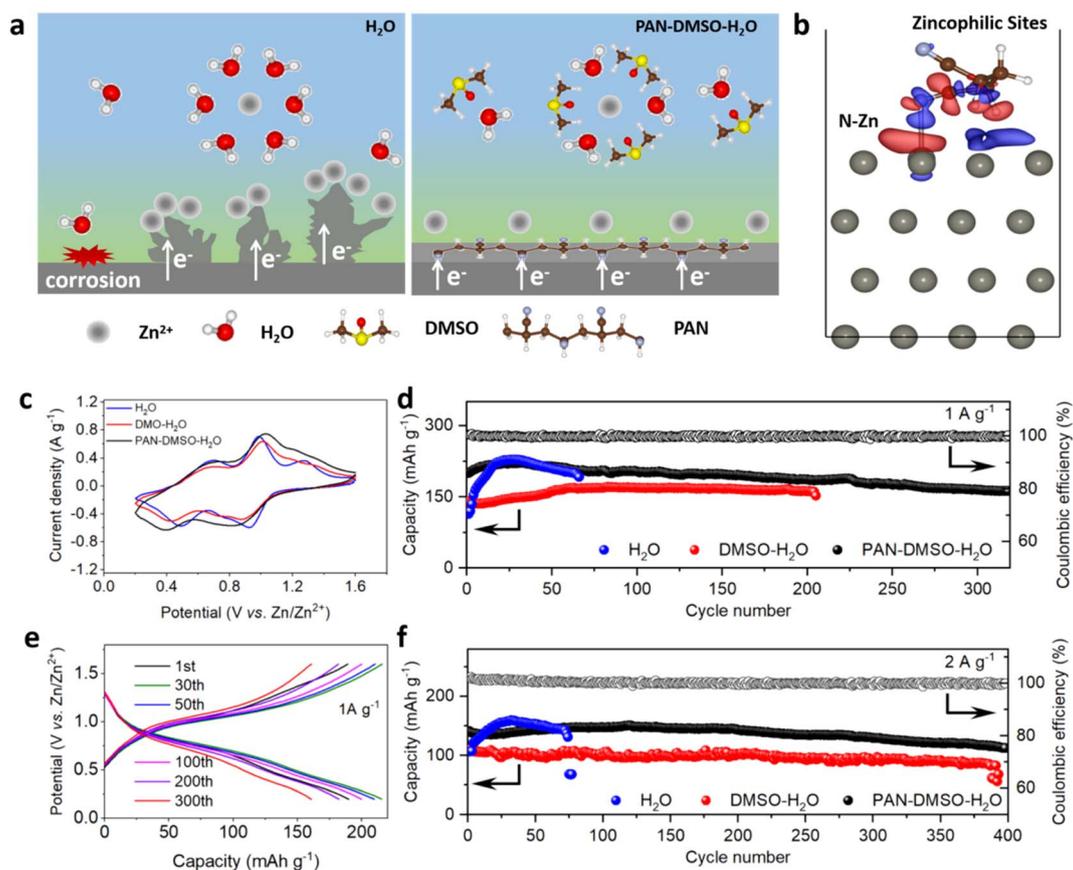

Fig. 5 (a) Schematic illustration of Zn deposition with the pristine aqueous (left) and PAN–DMSO–H$_2$O (right) electrolytes. (b) Side view of the charge density difference at the Zn–PAN interface. (c) CV profiles at a scan rate of 0.1 mV s^{-1} in different electrolytes. (d) Cycling performance at a current density of 1 A g^{-1} and (e) the corresponding galvanostatic charge–discharge curves. (f) Cycling performance at a current density of 2 A g^{-1}.

batteries either experience sudden failure or demonstrate a lower capacity in the pristine aqueous (Fig. S16a†) and DMSO–H_2O (Fig. S16b†) electrolytes during cycling. We believe such instabilities are mainly due to the failure of the Zn anode, since the performance of the Zn–NVO battery can be restored, and the cycling test continued, after replacement by a new anode, as shown in Fig. S16c.† As expected, with the help of the PAN–DMSO–H_2O electrolyte in inhibiting dendrite growth, the Zn–NVO battery can realize an outstanding cycling stability over 400 cycles at a current density of 2.0 A g^{-1} (Fig. 5f), which is comparable with many AZIBs.[62,63]

Conclusion

In summary, a novel aqueous electrolyte containing PAN and DMSO has been developed to protect a Zn anode from corrosion and dendrite growth, enabling the construction of high-performance AZIBs. After its solubilization by the DMSO in the electrolyte, the PAN can preferentially adsorb on the Zn anode surface and provide zincophilic sites to realize a uniform electric field. This is favorable for homogeneous Zn plating/stripping, leading to a smooth and dendrite-free anode surface. Moreover, the DMSO can regulate the solvation structure of the Zn^{2+} ions, which concurrently inhibits the side reactions and enhances the ion transport, further ensuring a dendrite-free Zn anode. Thanks to the synergistic effects of the PAN–DMSO–H_2O electrolyte, the Zn–Zn symmetric battery achieves enhanced coulombic efficiency (99.18%) and cycle life (more than 1200 h) at a current density of 5.0 mA cm^{-2}. Moreover, a Zn–NVO full battery with this PAN–DMSO–H_2O electrolyte exhibits an excellent capacity retention of 81.1% after 300 cycles. The results reported herein will inspire the development of other multifunctional electrolytes for dendrite-free Zn anodes in AZIBs.

Data availability

The data that supports this study is available from the corresponding ESI.†

Author contributions

Z. L. and Y. H. proposed the concept and supervised the work; Z. L., X. L., D. Wu and B. C. carried out the experimental design, characterization and electrochemical measurements; H. Wu. and P. H. prepared the cathode materials; J. M. and Z. L. performed the calculations; Z. L., J. M., Y. H., Z. L., L. W and S. C wrote and edited the manuscript; all authors helped to discuss the experimental data and theoretical results. Dr Z. L. and Dr J. M. contributed equally to this work.

Conflicts of interest

The authors declare no competing financial interest.

References

1 J. Cao, D. Zhang, X. Zhang, Z. Zeng, J. Qin and Y. Huang, *Energy Environ. Sci.*, 2022, **15**, 499–528.

2 L. E. Blanc, D. Kundu and L. F. Nazar, *Joule*, 2020, **4**, 771–799.

3 H. Tang, Y. Yin, Y. Huang, J. Wang, L. Liu, Z. Hu, H. Zhang, Y. Li, M. Zhu and O. G. Schmidt, *ACS Energy Lett.*, 2021, **6**, 1859–1868.

4 Y. Li, M. Zhu, V. K. Bandari, D. D. Karnausheko, D. Karnausheko, F. Zhu and O. G. Schmidt, *Adv. Energy Mater.*, 2022, **12**, 2103641.

5 S. Luo, L. Xie, F. Han, W. Wei, Y. Huang, H. Zhang, M. Zhu, O. G. Schmidt and L. Wang, *Adv. Funct. Mater.*, 2019, **29**, 1901336.

6 Y. Liu, Z. Dai, W. Zhang, Y. Jiang, J. Peng, D. Wu, B. Chen, W. Wei, X. Chen, Z. Liu, Z. Wang, F. Han, D. Ding, L. Wang, L. Li, Y. Yang and Y. Huang, *ACS Nano*, 2021, **15**, 9065–9075.

7 Y. Liu, Y. Jiang, Z. Hu, J. Peng, W. Lai, D. Wu, S. Zuo, J. Zhang, B. Chen, Z. Dai, Y. Yang, Y. Huang, W. Zhang, W. Zhao, W. Zhang, L. Wang and S. Chou, *Adv. Funct. Mater.*, 2021, **31**, 2008033.

8 W. Lu, C. Zhang, H. Zhang and X. Li, *ACS Energy Lett.*, 2021, **6**, 2765–2785.

9 J. Yang, B. Yin, Y. Sun, H. Pan, W. Sun, B. Jia, S. Zhang and T. Ma, *Nano-Micro Lett.*, 2022, **14**, 42.

10 M. Zhou, Y. Chen, G. Fang and S. Liang, *Energy Storage Mater.*, 2022, **45**, 618–646.

11 W. Zhang, J. Peng, W. Hua, Y. Liu, J. Wang, Y. Liang, W. Lai, Y. Jiang, Y. Huang, W. Zhang, H. Huang, Y. Yang, L. Li, Z. Liu, L. Wang and S. Chou, *Adv. Funct. Mater.*, 2021, **11**, 2100757.

12 Z. Liu, Z. Zhao, W. Zhang, Y. Huang, Y. Liu, D. Wu, L. Wang and S. Chou, *InfoMat*, 2022, **4**, e12260.

13 Y. Liu, J. Hu, Q. Lu, M. Hantusch, H. Zhang, Z. Qu, H. Tang, H. Dong, O. G. Schmidt, R. Holze and M. Zhu, *Energy Storage Mater.*, 2022, **47**, 98–104.

14 Q. Zhang, J. Luan, Y. Tang, X. Ji and H. Wang, *Angew. Chem., Int. Ed.*, 2020, **59**, 13180–13191.

15 D. Wang, Q. Li, Y. Zhao, H. Hong, H. Li, Z. Huang, G. Liang, Q. Yang and C. Zhi, *Adv. Energy Mater.*, 2022, **12**, 2102707.

16 Q. Yang, Q. Li, Z. Liu, D. Wang, Y. Guo, X. Li, Y. Tang, H. Li, B. Dong and C. Zhi, *Adv. Mater.*, 2020, **32**, 2001854.

17 M. Li, Z. Li, X. Wang, J. Meng, X. Liu, B. Wu, C. Han and L. Mai, *Energy Environ. Sci.*, 2021, **14**, 3796–3839.

18 H. Zhang, Z. Qu, H. Tang, X. Wang, R. Koehler, M. Yu, C. Gerhard, Y. Yin, M. Zhu, K. Zhang and O. G. Schmidt, *ACS Energy Lett.*, 2021, **6**, 2491–2498.

19 K. Guan, L. Tao, R. Yang, H. Zhang, N. Wang, H. Wan, J. Cui, J. Zhang, H. Wang and H. Wang, *Adv. Energy Mater.*, 2022, **12**, 2103557.

20 L. Yuan, J. Hao, C.-C. Kao, C. Wu, H.-K. Liu, S.-X. Dou and S.-Z. Qiao, *Energy Environ. Sci.*, 2021, **14**, 5669–5689.

21 J. Hao, X. Li, X. Zeng, D. Li, J. Mao and Z. Guo, *Energy Environ. Sci.*, 2020, **13**, 3917–3949.

22 X.-S. Lin, Z.-R. Wang, L.-H. Ge, J.-W. Xu, W.-Q. Ma, M.-M. Ren, W.-L. Liu, J.-S. Yao and C.-B. Zhang, *ChemElectroChem*, 2022, **9**, e202101724.

23 M. Xi, Z. Liu, J. Ding, W. Cheng, D. Jia and H. Lin, *ACS Appl. Mater. Interfaces*, 2021, **13**, 29631–29640.

24 A. Bayaguud, X. Luo, Y. Fu and C. Zhu, *ACS Energy Lett.*, 2020, **5**, 3012–3020.

25 S.-J. Zhang, J. Hao, D. Luo, P.-F. Zhang, B. Zhang, K. Davey, Z. Lin and S.-Z. Qiao, *Adv. Energy Mater.*, 2021, **11**, 2102010.

26 X. Guo, Z. Zhang, J. Li, N. Luo, G.-L. Chai, T. S. Miller, F. Lai, P. Shearing, D. J. L. Brett, D. Han, Z. Weng, G. He and I. P. Parkin, *ACS Energy Lett.*, 2021, **6**, 395–403.

27 R. Yao, L. Qian, Y. Sui, G. Zhao, R. Guo, S. Hu, P. Liu, H. Zhu, F. Wang, C. Zhi and C. Yang, *Adv. Energy Mater.*, 2021, **12**, 2102780.

28 J. Zhao, J. Zhang, W. Yang, B. Chen, Z. Zhao, H. Qiu, S. Dong, X. Zhou, G. Cui and L. Chen, *Nano Energy*, 2019, **57**, 625–634.

29 L. Zhang, L. Miao, W. Xin, H. Peng, Z. Yan and Z. Zhu, *Energy Storage Mater.*, 2022, **44**, 408–415.

30 Y. Zhong, Z. Cheng, H. Zhang, J. Li, D. Liu, Y. Liao, J. Meng, Y. Shen and Y. Huang, *Nano Energy*, 2022, **98**, 107220.

31 W. Xu, K. Zhao, W. Huo, Y. Wang, G. Yao, X. Gu, H. Cheng, L. Mai, C. Hu and X. Wang, *Nano Energy*, 2019, **62**, 275–281.

32 P. Sun, L. Ma, W. Zhou, M. Qiu, Z. Wang, D. Chao and W. Mai, *Angew. Chem., Int. Ed.*, 2021, **133**, 18395–18403.

33 Y. Xu, X. Zhang, J. Sun, W. Wang, M. Wang, Y. Yuan, M. Chuai, N. Chen, H. Hu and W. Chen, *Nano Lett.*, 2022, **22**, 3298–3306.

34 Q. Zhang, J. Luan, L. Fu, S. Wu, Y. Tang, X. Ji and H. Wang, *Angew. Chem., Int. Ed.*, 2019, **131**, 15988–15994.

35 Y. Jin, K. S. Han, Y. Shao, M. L. Sushko, J. Xiao, H. Pan and J. Liu, *Adv. Funct. Mater.*, 2020, **30**, 2003932.

36 M. Yan, C. Xu, Y. Sun, H. Pan and H. Li, *Nano Energy*, 2021, **82**, 105739.

37 X. Zhou, Y. Lu, Q. Zhang, L. Miao, K. Zhang, Z. Yan, F. Li and J. Chen, *ACS Appl. Mater. Interfaces*, 2020, **12**, 55476–55482.

38 S. J. Banik and R. Akolkar, *J. Electrochem. Soc.*, 2013, **160**, D519.

39 M. Yan, N. Dong, X. Zhao, Y. Sun and H. Pan, *ACS Energy Lett.*, 2021, **6**, 3236–3243.

40 D. Feng, F. Cao, L. Hou, T. Li, Y. Jiao and P. Wu, *Small*, 2021, **17**, 2103195.

41 L. Cao, D. Li, E. Hu, J. Xu, T. Deng, L. Ma, Y. Wang, X.-Q. Yang and C. Wang, *J. Am. Chem. Soc.*, 2020, **142**, 21404–21409.

42 R. Feng, X. Chi, Q. Qiu, J. Wu, J. Huang, J. Liu and Y. Liu, *ACS Appl. Mater. Interfaces*, 2021, **13**, 40638–40647.

43 H. Du, K. Wang, T. Sun, J. Shi, X. Zhou, W. Cai and Z. Tao, *Chem. Eng. J.*, 2022, **427**, 131705.

44 F. Ming, Y. Zhu, G. Huang, A.-H. Emwas, H. Liang, Y. Cui and H. N. Alshareef, *J. Am. Chem. Soc.*, 2022, **144**, 7160–7170.

45 Y. Fang, X. Xie, B. Zhang, Y. Chai, B. Lu, M. Liu, J. Zhou and S. Liang, *Adv. Funct. Mater.*, 2022, **32**, 2109671.

46 P. Chen, X. Yuan, Y. Xia, Y. Zhang, L. Fu, L. Liu, N. Yu, Q. Huang, B. Wang, X. Hu, Y. Wu and T. V. Ree, *Adv. Sci.*, 2021, **8**, 2100309.

47 A. Panuszko, P. Bruździak, M. Śmiechowski, M. Stasiulewicz, J. Stefaniak and J. Stangret, *J. Mol. Liq.*, 2019, **294**, 111661.

48 R. L. Mancera, M. Chalaris and J. Samios, *J. Mol. Liq.*, 2004, **110**, 147.

49 Q. Zhang, Y. Lu, L. Miao, Q. Zhao, K. Xia, J. Liang, S.-L. Chou and J. Chen, *Angew. Chem., Int. Ed.*, 2018, **57**, 14796–14800.

50 Q. Li, Y. Zhao, F. Mo, D. Wang, Q. Yang, Z. Huang, G. Liang, A. Chen and C. Zhi, *EcoMat*, 2020, **2**, e12035.

51 F. Xie, H. Li, X. Wang, X. Zhi, D. Chao, K. Davey and S. Qiao, *Adv. Energy Mater.*, 2021, **11**, 2003419.

52 X. Wu and A. Liu, *Chem. J. Chin. Univ.*, 2017, **12**, 2220.

53 H. G. M. Edwards, A. R. Hoskins, A. F. Johnson and I. R. Lewis, *Polym. Int.*, 1993, **30**, 25–32.

54 M. Zhu, S. Guo, J. Li, X. Luo, Z. Liu, T. Zhang, X. Cao, M. Long, B. Lu, A. Pan, G. Fang, J. Zhou and S. Liang, *Adv. Mater.*, 2021, **33**, 2100187.

55 Z. Miao, Q. Liu, W. Wei, X. Zhao, M. Du, H. Li, F. Zhang, M. Hao, Z. Cui, Y. Sang, X. Wang, H. Liu and S. Wang, *Nano Energy*, 2022, **97**, 107145.

56 K. Zhao, G. Fan, J. Liu, F. Liu, J. Li, X. Zhou, Y. Ni, M. Yu, Y. Zhang, H. Su, Q. Liu and F. Cheng, *J. Am. Chem. Soc.*, 2022, **144**, 11129–11137.

57 N. Liu, X. Wu, Y. Zhang, Y. Yin, C. Sun, Y. Mao, L. Fan and N. Zhang, *Adv. Sci.*, 2020, **7**, 2000146.

58 Z.-W. Wu, S.-L. Tyan, H.-H. Chen, J.-C.-A. Huang, Y.-C. Huang, C.-R. Lee and T.-S. Mo, *Superlattices Microstruct.*, 2017, **107**, 38–43.

59 Y. An, Y. Tian, K. Zhang, Y. Liu, C. Liu, S. Xiong, J. Feng and Y. Qian, *ACS Nano*, 2021, **15**, 15259–15273.

60 C. Huang, X. Zhao, S. Liu, Y. Hao, Q. Tang, A. Hu, Z. Liu and X. Chen, *Adv. Mater.*, 2021, **33**, 2100445.

61 H.-Y. Wu, X. Gu, P. Huang, C. Sun, H. Hu, Y. Zhong and C. Lai, *J. Mater. Chem. A*, 2021, **9**, 7025–7033.

62 F. Wan, L. Zhang, X. Dai, X. Wang, Z. Niu and J. Chen, *Nat. Commun.*, 2018, **9**, 1656.

63 D. Liu, Y. Zhang, S. Liu, L. Wei, S. You, D. Chen, M. Ye, Y. Yang, X. Rui, Y. Qin and C. C. Li, *Adv. Funct. Mater.*, 2022, **32**, 2111714.